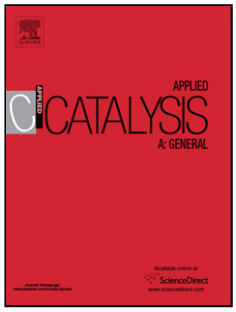

Title: Well-Controlled Radical-Based Epoxidation Catalyzed by Copper Complex Immobilized on Bipyridine-Periodic Mesoporous Organosilica

Authors: Satoshi Ishikawa, Yoshifumi Maegawa, Minoru Waki, Shinji Inagaki

PII: S0926-860X(19)30062-6
DOI: https://doi.org/10.1016/j.apcata.2019.02.007
Reference: APCATA 16977

To appear in: *Applied Catalysis A: General*

Received date: 29 December 2018
Revised date: 1 February 2019
Accepted date: 5 February 2019

Please cite this article as: Ishikawa S, Maegawa Y, Waki M, Inagaki S, Well-Controlled Radical-Based Epoxidation Catalyzed by Copper Complex Immobilized on Bipyridine-Periodic Mesoporous Organosilica, *Applied Catalysis A, General* (2019), https://doi.org/10.1016/j.apcata.2019.02.007

Well-Controlled Radical-Based Epoxidation Catalyzed by Copper Complex Immobilized on Bipyridine-Periodic Mesoporous Organosilica

Satoshi Ishikawa,[a,‡] Yoshifumi Maegawa,[a] Minoru Waki,[a] and Shinji Inagaki*[a]

[a] Toyota Central R&D Labs., Inc., Nagakute, Aichi 480-1192, Japan.

E-mail: inagaki@mosk.tytlabs.co.jp

Graphical Abstract

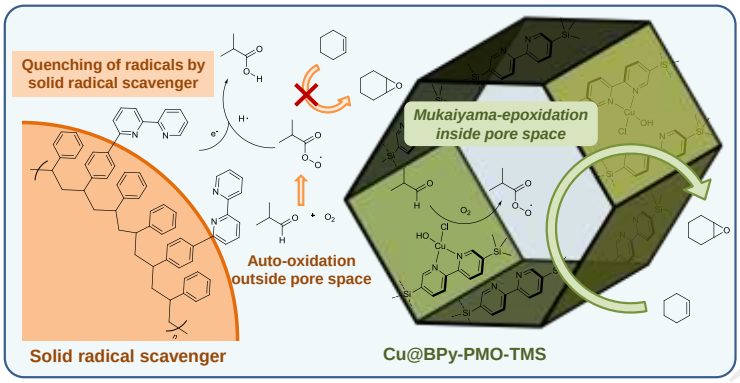

Highlights

A new concept for a safe radical reaction system

Cu-bipyridine catalyst was directly formed on the pore surfaces of BPy-PMO

The catalyst exhibited good catalytic activity and reusability for epoxidation

Addition of solid scavenger allowed the reaction solely inside the mesopore space

Abstract

The development of synthetic methods and reaction systems for safe radical reactions is of extremely industrial importance. Here we proposed new concept for a safe radical reaction system based on combined use of a mesoporous catalyst and an insoluble solid scavenger. We selected Mukaiyama epoxidation of olefin as a model radical reaction and investigated the catalysis of Cu-bipyridine complexes immobilized on trimethylsilylated bipyridine-periodic mesoporous organosilica as a solid support. The immobilized Cu complex exhibited high

catalytic activity and reusability for Mukaiyama epoxidation at low substrate concentration (1 mmol) but free-radical auto-oxidation also occurred at high substrate concentration (7 mmol). Although both epoxidation reactions outside and inside the mesochannels were almost completely quenched by addition of molecular scavenger, addition of solid scavenger allowed quenching the reaction outside the mesopores but not inside the mesopores because the solid scavenger could not access the interior of the mesochannels. Thus, the combined use of a mesoporous catalyst and a solid radical scavenger would offer new reaction system for safe radical reactions.

Keywords: mesoporous materials; metal complex catalysts; radical reactions; Mukaiyama epoxidation

1. Introduction

Radical reactions have attracted much attention because radicals can react with most organic molecules and afford reaction products such as sterically hindered molecules and unique polymers that cannot be synthesized by typical catalytic reactions [1]. The utilization of radicals for organic reactions is expected to expand the scope of organic synthesis. However, radicals are sometimes too active in nature and can cause thermal runaway, fire, and explosions [2,3].

Product selectivity is sometimes low due to the undesired side reactions. Therefore, the development of synthetic methods and reaction systems for safe radical reactions has been highly desirable.

Ramos-Fernandez *et al.* reported the titania-catalyzed oxidative dehydrogenation of ethyl lactate based on a free-radical reaction mechanism [4]. To improve the product yield and minimize by-product formation, the reaction was performed in the presence of activated carbon as a solid radical scavenger. The solid radical scavenger efficiently hampered the formation of undesired products in the solution without a loss of catalysis on TiO_2 for the desired reaction. This unique strategy encouraged us to examine the radical reaction using a heterogeneous metal catalyst and a solid radical scavenger.

We recently reported the preparation of a periodic mesoporous organosilica including 2,2'-bipyridine (BPy) ligands within the framework (BPy-PMO, Fig. 1) [5]. BPy-PMO has a highly ordered mesoporous structure with a unique pore wall structure, in which BPy ligands are densely and regularly packed, and exposed on the pore surfaces. BPy ligands have high coordination ability; therefore, various metal-bipyridine complexes (e.g. Ir, Ru, Rh, and Mo, etc) can be formed directly on the pore surfaces of BPy-PMO [6-10]. The metal complex-immobilized BPy-PMOs exhibit efficient heterogeneous catalysis for various reactions including direct C-H borylation of arenes [5,6], selective oxidation of alkanes [7], water

oxidation [8], transfer hydrogenation of nitrogen heterocycles [9], and epoxidation of olefins [10]. However, there have been no reports on radical-based reactions using BPy-PMO as a catalyst support.

Here, we report the immobilization of a Cu complex on BPy-PMO and application to a radical-based epoxidation reaction (Mukaiyama epoxidation [11-13]). A Cu-bipyridine complex was formed on the pore surfaces of BPy-PMO by reaction with $CuCl_2$. The Cu complex immobilized on BPy-PMO exhibits efficient catalysis for the Mukaiyama epoxidation of cyclohexene with molecular oxygen in the presence of isobutyraldehyde. End-capping of the surface silanol groups with trimethylsilyl groups was very effective to improve the activity and recyclability for Mukaiyama epoxidation. Although the Mukaiyama epoxidation proceeded efficiently at low substrate concentration (1 mmol), the radical auto-oxidation reaction occurred at high substrate concentration (7 mmol), even in the absence of the catalyst. Polystyrene-supported bipyridine (PS-BPy) beads were added as a solid radical scavenger to control the undesired side reaction. The addition of the solid radical scavenger quenched the reaction in the solution but did not quench the reaction inside the mesopore spaces of BPy-PMO (Fig. 1). The combined use of a solid scavenger and a mesoporous catalyst may lead to the possibility of controllable radical reactions.

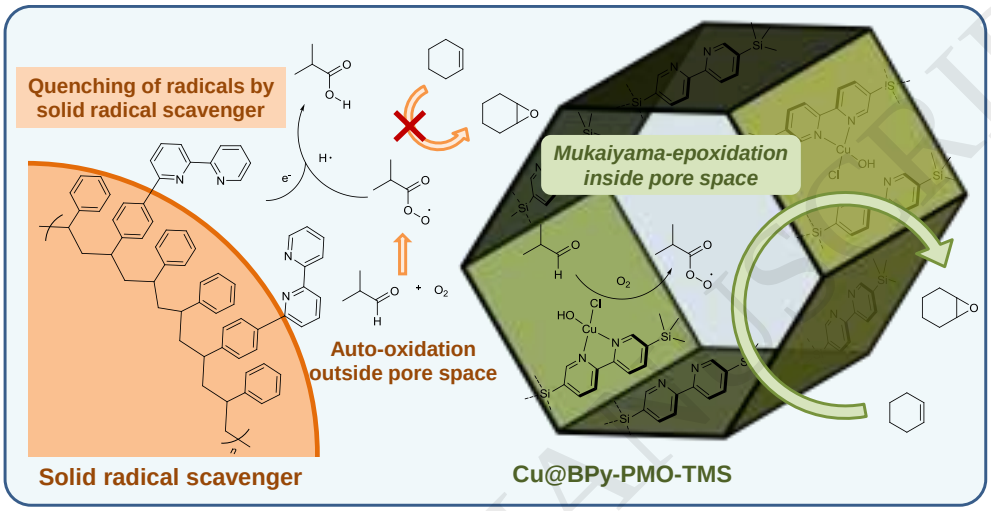

Fig. 1. Schematic image of the copper-immobilized BPy-PMO nanoreactor for Mukaiyama epoxidation in combination with a solid radical scavenger.

2. Experimental methods

2.1. Materials and methods

BPy-PMO and end-capped BPy-PMO with trimethylsilyl groups (BPy-PMO-TMS) were prepared according to the literature, respectively [5]. PS-BPy beads (100–200 mesh, Fig. S1, see Supplementary Material) were purchased from Sigma-Aldrich. All other chemicals were commercially available and were used without purification. Gas chromatography-mass spectrometry (GC-MS; Agilent 6890GC/5973MSD) analyses were performed using a flame ionization detector (FID) and a capillary column (HP-5MS, 0.25 mm × 30 m). Nitrogen adsorption experiments were performed on a Nova3000e (Quantachrome) at liquid nitrogen temperature. Pore-size distribution curves were calculated using the density functional theory (DFT) (DFT kernel: silica, cylindrical pores, nonlinear DFT (NLDFT) equilibrium model). Specific surface areas were calculated from the linear regions of Brunauer-Emmett-Teller (BET) plots (P/P_0 = 0.1–0.25). The *t*-plot method was applied to estimate the pore volumes. Powder X-ray diffraction (XRD) measurements were performed on a Rigaku RINT-TTR with Cu-Kα radiation (50 kV, 300 mA). Scanning electron microscopy (SEM) measurements were performed on a Hitachi S-3600N equipped with energy dispersive X-ray spectroscopy (EDX) detector. Ultraviolet-visible (UV-vis) spectroscopy measurements were performed on a Jasco V-670 spectrophotometer. X-ray absorption fine structure (XAFS) measurements at the Cu *K*-edge were performed at the BL14B2 beamline of SPring-8 and the data were collected in transmission mode. Synchrotron radiation X-rays were monochromatized by a Si(311)

double-crystal monochromator. Ion chambers were placed front and behind the samples to detect the intensity of incident and transmitted X-rays (I_0 and I, respectively). Background reduction was conducted using the Autobk and Spline smoothing algorithm. The κ^3-weighted extended XAFS (EXAFS) oscillations (2.0-12 Å) were Fourier transformed into *R*-space. The EXAFS data was fitted in *R*-space (1.5-2.2 Å). The fitting parameters were the coordination number (CN), the interatomic distance (*R*), the correction-of-edge energy (ΔE_0), and the Debye-Waller factor (σ^2). Backscattering amplitudes and Phase-shift were calculated using the FEFF6 code.

2.2. Formation of Cu complexes on BPy-PMOs

To a suspension of BPy-PMO (47.8 mg, 0.15 mmol) or BPy-PMO-TMS (68.5 mg, 0.20 mmol) in acetonitrile (8 mL) was added a solution of $CuCl_2$ in acetonitrile (10 mM, 2 mL, 0.02 mmol). The reaction mixture was then stirred (500 rpm) at room temperature for 24 h. The obtained powder was filtered, washed with acetonitrile, and dried under reduced pressure to give Cu-BPy-PMO or Cu-BPy-PMO-TMS.

2.3. Catalytic reaction

To a solution of cyclohexene (0.10 mL, 1.0 mmol), isobutyraldehyde (0.27 mL, 3.0

mmol) and chloroform (9.62 mL) was added Cu-BPy-PMO (20 mg) or Cu-BPy-PMO-TMS (20 mg). The reaction flask as then set in an oil bath kept at 40 °C. After attaching a balloon filled with 1 L of oxygen, the reaction was started. Aliquots of the reaction solution were collected periodically and centrifuged to separate the solid materials. The supernatant was then mixed with a known amount of toluene as an external standard for analysis by GC (GC-8A, Shimadzu) with a flame ionization detector (FID) and a capillary column (HP-5, 0.53 mm × 30 m). After the reaction was completed, the solid catalyst was filtered, washed with acetonitrile, and dried under evacuation. The recovered catalyst was then reused in the next reaction under the same conditions.

3. Results and discussion

3.1. Immobilization of Cu complex on BPy-PMO

To immobilize Cu complexes on the pore surfaces, BPy-PMO powder was dispersed in acetonitrile, methanol, or deionized water containing $CuCl_2$ and then stirred at room temperature for 24 h. XRD patterns of the recovered Cu-immobilized BPy-PMOs were measured to confirm whether the ordered mesoporous structure of BPy-PMO was preserved or not. The ordered mesoporous structure was preserved when acetonitrile was used as a solvent. The XRD pattern showed a peak at $2\theta = 1.78°$ due to the ordered mesostructure and also peaks at $2\theta = 7\text{-}35°$ due to the periodic arrangement of the bipyridine groups in the pore walls, similar to those of the original BPy-PMO (Fig. 2). However, the mesoporous structure was collapsed when methanol or deionized water were used as solvents (Fig. S2, see Supplementary Material). BPy-PMO powder was stirred in methanol or deionized water without the addition of $CuCl_2$ to check the stability of BPy-PMO in these solvents. As a result, the ordered mesoporous and pore wall structures were completely preserved, which indicates that the presence of $CuCl_2$ in protic solvents such as methanol and deionized water would damage the mesoporous structure. BPy-PMO-TMS was also treated with $CuCl_2$ in acetonitrile. The XRD pattern of Cu-BPy-PMO-TMS was almost the same as that of the pristine BPy-PMO-TMS, which indicates the preservation of both the ordered mesoporous structure and the molecular-scale periodicity in the pore walls (Fig. 2).

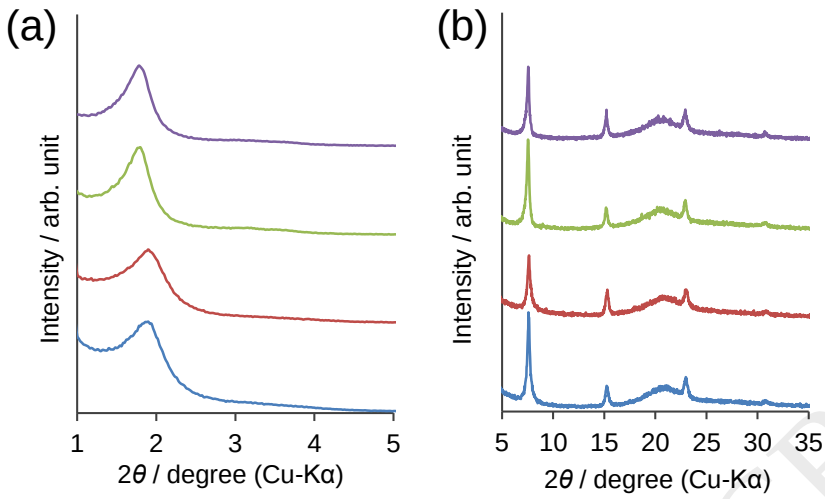

Fig. 2. (a) Low and (b) medium scattering-angle XRD patterns of BPy-PMO (blue line), Cu-BPy-PMO (red line), BPy-PMO-TMS (green line), and Cu-BPy-PMO-TMS (purple line).

Fig. 3 shows nitrogen adsorption/desorption isotherms for BPy-PMO and BPy-PMO-TMS before and after immobilization of the Cu complexes. All were typical type IV isotherms, which indicate the presence of uniform mesoporosity, although the adsorption amounts decreased after the formation of Cu complexes on the pore surfaces. Table 1 lists the BET surface areas (S_{BET}), density functional theory pore diameters (d_{DFT}) and mesopore volumes (V_p) of Cu-immobilized BPy-PMO and BPy-PMO-TMS. Cu-BPy-PMO and Cu-BPy-PMO-TMS have high S_{BET} of 573 and 597 m^2 g^{-1}, and d_{DFT} of 4.1 and 3.8 nm, respectively, which were almost the same or slightly smaller than those of pristine BPy-PMO and BPy-PMO-TMS, respectively.

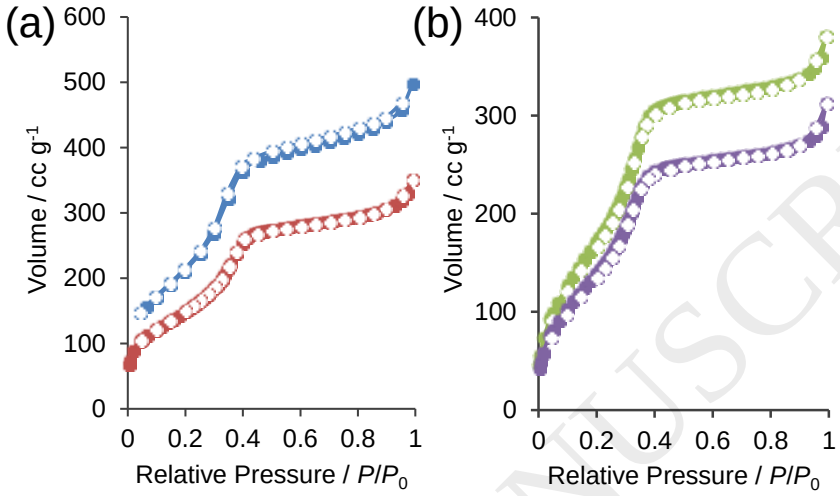

Fig. 3. Nitrogen adsorption/desorption isotherms of (a) BPy-PMO (blue line) and Cu-BPy-PMO (red line), (b) BPy-PMO-TMS (green line), and Cu-BPy-PMO-TMS (purple line). Closed circles, adsorption; open circles, desorption.

The amounts of Cu loading were measured using EDX and are listed in Table 1. EDX analysis showed that the Cu/Si atomic ratios were 0.07 and 0.04 for Cu-BPy-PMO and Cu-BPy-PMO-TMS, respectively. The Si/BPy molar ratio was 2/1 for BPy-PMO and 10/3 for BPy-PMO-TMS [5]; therefore, the molar ratios of Cu to the total BPy ligands (Cu/BPy) were calculated to be 0.14 and 0.13, respectively (assuming that the silanol groups (Si-OH) at the pore surfaces (2/3 of the total Si) were completely trimethylsilylated for BPy-PMO-TMS [5]).

The Cu complexes are formed only on the BPy ligands exposed on the surface because the pore walls are composed of three layers of Si-BPy-Si units. Thus, the molar ratio of Cu to the surface BPy ligands (Cu/BPy_{surf}) were 0.21 and 0.20 for Cu-BPy-PMO and Cu-BPy-PMO-TMS, respectively, which indicates that approximately 20% of the surface BPy ligands coordinate with Cu. The Cl/Cu atomic ratios were 1.0 for both samples, which were apparently lower that of the ideal ratio of 2 ($CuCl_2$). This indicates the loss of Cl anions during the metalation process.

Table 1. Physical parameters of Cu-immobilized BPy-PMO and BPy-PMO-TMS

Sample	S_{BET}[a] $m^2\ g^{-1}$	d_{DFT}[a] nm	V_p[a] cc g^{-1}	Cu/Si[b]	Cu/BPy_{surf}[b]	Cl/Cu[b]
BPy-PMO	693	4.3	0.50	-	-	-
Cu-BPy-PMO	573	4.1	0.38	0.07	0.23	1.0
BPy-PMO-TMS	654	3.8	0.41	-	-	-
Cu-BPy-PMO-TMS	597	3.8	0.36	0.04	0.22	1.0

[a]Measured by N_2 adsorption at liquid N_2 temperature (-196 °C). S_{BET} calculated by the BET method. d_{DFT} calculated by the DFT method. V_p calculated by the *t*-plot method. [b]Estimated from EDX measurement. Cu/BPy_{surf} calculated by taking into account the following assumptions: (1) the crystal wall of BPy is composed of three layers; (2) the Si/BPy ratio in the

crystal wall is 2 in BPy-PMO, and (3) 10/3 in BPy-PMO-TMS.

The electronic structure of the Cu-bipyridine complex in Cu-BPy-PMO and Cu-BPy-PMO-TMS was evaluated using UV-vis spectroscopy. Fig. S3 shows UV-vis absorption spectra for Cu-BPy-PMO and BPy-PMO-TMS together with $Cu(bpy)Cl_2$ as a model complex [14]. $Cu(bpy)Cl_2$ exhibited an absorption centred at 710 nm, which is attributable to the *d-d* transitions of Cu^{2+} in a tetragonally distorted octahedral configuration [15,16]. Cu-BPy-PMO and Cu-BPy-PMO-TMS showed a broad absorption centred at 770 nm. The peak broadening and red-shift of the absorption band compared with that for $Cu(bpy)Cl_2$ may be due to the changes in electronic state of Cu^{2+} by the attachment of silicon atoms at both sides of the bipyridine ligand [17]. Similar changes in UV-vis spectra were observed in other metal-immobilized BPy-PMO.[5] Cu-BPy-PMO also had a shoulder peak at 980 nm. Taking into account there was no absorption in Cu-BPy-PMO-TMS, the additional absorption may be caused by the formation of an unidentified copper complex by reaction between the silanol groups and $CuCl_2$.

The coordination state of the copper centres in Cu-BPy-PMO and Cu-BPy-PMO-TMS were studied using XAFS measurements. X-ray absorption near-edge spectroscopy (XANES) measurements at the Cu *K*-edge of Cu-BPy-PMO and Cu-BPy-PMO-TMS showed a

characteristic weak peak attributable to the 1s→3d transition at 8977 eV, as well as that for $Cu(bpy)Cl_2$ (Fig. S4, see Supplementary Material). The absorption edge in the rising part was observed at 8985.2, 8984.6, and 8984.9 eV for Cu-BPy-PMO, Cu-BPy-PMO-TMS, and $Cu(bpy)Cl_2$, respectively. The chemical shifts relative to the *K*-edge energy of Cu foil (8979 eV) were 5.6-6.2 eV, which is characteristic value of +2 oxidation state of the copper centre.

Curve-fitting analyses of EXAFS Fourier transforms were conducted using the available crystal structure of $Cu(bpy)Cl_2$ as a model complex to generate the theoretical model (Figs. S5-6, see Supplementary Material) [18]. The radial structural functions of Cu-BPy-PMO-TMS were almost fitted to the model structure by adopting the crystal structural parameter of $Cu(bpy)Cl_2$ (Table S1, see Supplementary Material). However, the EXAFS Fourier transform of Cu-BPy-PMO showed deviation from the fitting curve under the same analytical conditions, which suggests that the local coordination structure of Cu-BPy-PMO may differ slightly from that of $Cu(bpy)Cl_2$, possibly due to the formation of an unidentified copper complex as observed for the UV-vis absorption spectra.

3.2. Mukaiyama epoxidation by Cu-immobilized BPy-PMO catalysts

The catalytic properties of Cu-BPy-PMO and Cu-BPy-PMO-TMS for Mukaiyama epoxidation with dioxygen were evaluated (Table 2). Cyclohexene and isobutyraldehyde were selected as

substrate and co-reagent, respectively. Under general epoxidation conditions, auto-oxidation occurs, even in the absence of a catalyst and especially at high substrate concentration. We confirmed that almost no reaction occurred within 150 min without a catalyst when 1 mmol of cyclohexene and 3 mmol of isobutyraldehyde were used in chloroform solvent under an oxygen atmosphere at 40 °C. Thus, the catalysis evaluation was conducted under the same conditions. 1,2-Epoxycyclohexane (**1**), 2-cyclohexene-1-ol (**2**), 2-cyclohexene-1-one (**3**) and 1,2-cyclohexanediol (**4**) were obtained as reaction products (Scheme 1). Among these products, the selectivity toward **1** was ca. 90% in all cases; therefore, only the yield of **1** was used for evaluation of the catalytic activity.

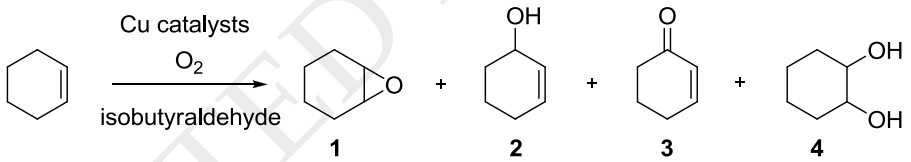

Scheme 1. Reaction scheme of Mukaiyama epoxidation of cyclohexene by catalyzed by Cu-BPy-PMO and Cu-BPy-PMO-TMS in the presence of O_2 and isobutyraldehyde.

Table 2. Mukaiyama epoxidation of cyclohexene catalyzed by Cu-BPy-PMO and Cu-BPy-PMO-TMS in the presence of O_2 and isobutyraldehyde.[a]

Catalyst	Conversion [%][b]	Selectivity [%][c]	Yield [%][d]	By-product selectivity [%][e]		
				2	**3**	**4**
Cu-BPy-PMO	7.3	89	6.5	2.5	6.4	1.9
Cu-BPy-PMO-TMS 1st reaction	17.3	89	15.6	2.6	8.6	0
Cu-BPy-PMO-TMS 2nd reaction	16.3	90	14.7	2.1	5.4	2.9
Cu-BPy-PMO-TMS 3rd reaction	22.8	92	21.0	2.0	4.0	2.0

[a] All reactions were conducted with cyclohexene (1 mmol) and isobutyraldehyde (3 mmol) in chloroform (10 mL) at 40 °C under oxygen (1 atm). [b] Conversion of cyclohexene. [c] Selectivity of **1** was calculated as yield of **1**/total yield of reaction products. [d] Yield of **1** based on cyclohexene. [e] Selectivity of by-products was calculated as yield of **2** or **3** or **4**/total yield of reaction products, respectively.

Fig. 4 shows reaction kinetic curves for the epoxidation of cyclohexene to **1**. In the absence of a catalyst, almost no product formation was observed. Likewise, almost no product was formed when BPy-PMO or BPy-PMO-TMS were used. However, the use of Cu-BPy-PMO promoted epoxidation without an induction period and the yield of **1** increased continuously with the reaction time. The product yield after 150 min was 6.5%, which corresponds to a turnover number (TON) of 9. Cu-BPy-PMO-TMS exhibited a higher reaction rate with a turnover frequency (TOF) within the initial 60 min (TOF = 14.4 h^{-1}) that was 4.3 times higher than that of Cu-BPy-PMO. The reaction proceeded continuously with the reaction time and the product yield reached 15.6% after 150 min, which corresponds to a TON of 30. The higher catalytic activity of Cu-BPy-PMO-TMS than that with Cu-BPy-PMO is considered to be for following reasons: (1) TMS treatment of the surface silanol groups contribute to smooth mass transfer within the mesochannels because oxygenated products such as epoxides tend to interact with the silanol groups. Such a promotion effect of diffusion by trimethylsilylation has been reported previously for mesoporous silica-based oxidation catalysts [19-23]. (2) The TMS treatment also excludes the formation of an undesired Cu complex by reaction between $CuCl_2$ and the silanol groups at the BPy-PMO surfaces, which was suggested by UV-vis absorption

spectra and EXAFS analysis.

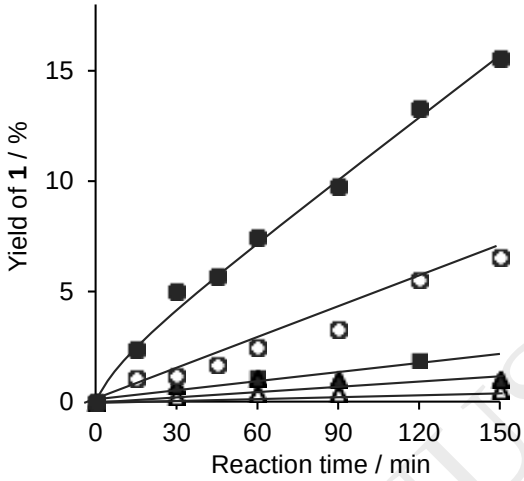

Fig. 4. Time dependent yield of **1** over Cu-BPy-PMO-TMS (closed circles), Cu-BPy-PMO (open circles), BPy-PMO-TMS (closed triangles), BPy-PMO (open triangles), and without catalyst (closed squares). All reactions were conducted with cyclohexene (1 mmol) and isobutyraldehyde (3 mmol) in chloroform (10 mL) at 40 °C under oxygen (1 atm).

Cu-BPy-PMO-TMS exhibited high reusability for Mukaiyama epoxidation. Cu-BPy-PMO-TMS was recovered by filtration under air and washed with solvent, followed by drying at 60 °C under reduced pressure. The recycle reactions were conducted under identical conditions. The recovered Cu-BPy-PMO-TMS exhibited almost no loss of activity and selectivity for at least two recycle uses (Fig. 5, Table 2).

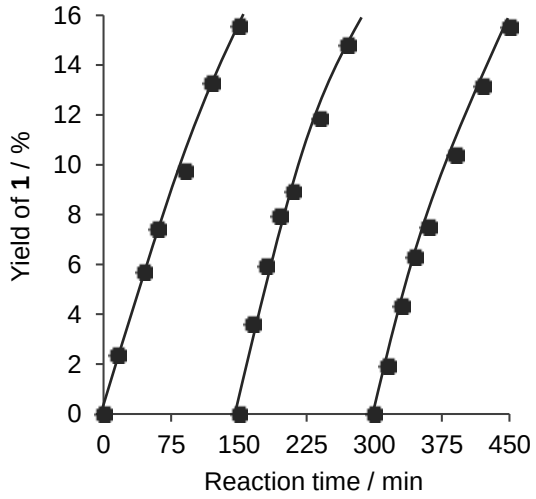

Fig. 5. Recycle experiment using Cu-BPy-PMO-TMS. All reactions were conducted with cyclohexene (1 mmol) and isobutyraldehyde (3 mmol) in chloroform (10 mL) at 40 °C under oxygen (1 atm) in the presence of Cu-BPy-PMO-TMS or recovered Cu-BPy-PMO-TMS.

Fig. 6 shows N_2 adsorption/desorption isotherms for Cu-BPy-PMO and Cu-BPy-PMO-TMS before and after the reactions. Cu-BPy-PMO showed a large decrease in the amount of adsorption after the first reaction, while Cu-BPy-PMO-TMS showed a very small decrease in the amount of adsorption, even after the third reaction. The BET surface areas of Cu-BPy-PMO and Cu-BPy-PMO-TMS after the first reaction were largely different at 141 and 543 $m^2\ g^{-1}$, respectively (Table S2). XRD analysis also showed that the low angle reflections due to the ordered mesoporous structure were retained for Cu-BPy-PMO-TMS, although they were largely decreased for Cu-BPy-PMO after the first reaction (Fig. S7, see Supplementary Material). These results indicate that Cu-BPy-PMO-TMS has higher structural stability than

Cu-BPy-PMO for Mukaiyama epoxidation. The improved structural stability by TMS treatment would also contribute to the high catalytic activity and high reusability.

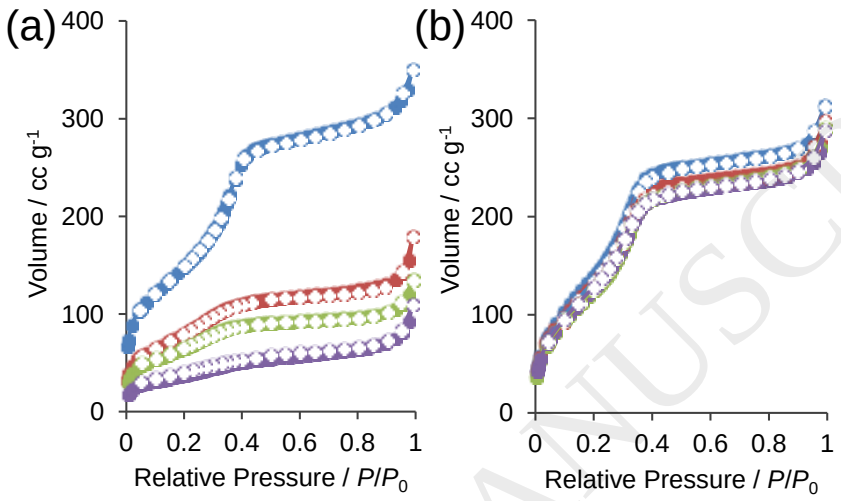

Fig. 6. Nitrogen adsorption/desorption isotherms for (a) Cu-BPy-PMO and (b) Cu-BPy-PMO-TMS before (blue line) and after the first (red line), second (green), and third reaction (purple line). Closed circles, adsorption; open circles, desorption.

Hot filtration experiments were also conducted to evaluate the leaching of copper species. Fig. 7 shows reaction kinetic curves before and after removal of the PMO catalyst when the reaction had proceeded for 60 min. No significant change in the product yield was observed after removal of the PMO catalyst, which indicates that the catalytic reaction occurred only over Cu-BPy-PMO-TMS.

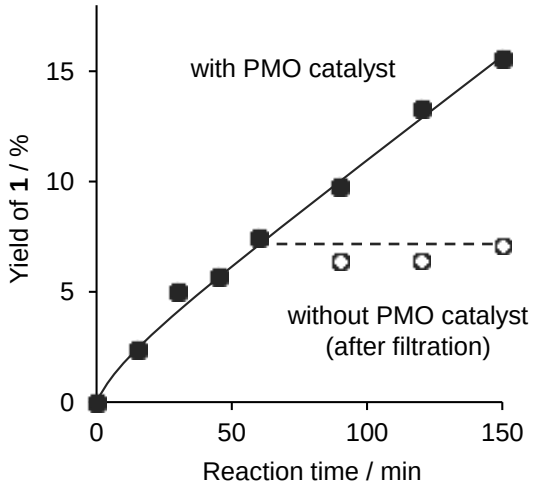

Fig. 7. Results of hot filtration experiments. Cu-BPy-PMO-TMS was removed at 60 min from the start of the reaction. Closed circles, time dependent yield of **1** without removal of the catalyst; open circles, time dependent yield of **1** after the removal of Cu-BPy-PMO-TMS. All reactions were conducted with cyclohexene (1 mmol) and isobutyraldehyde (3 mmol) in chloroform (10 mL) at 40 °C under oxygen (1 atm).

The molecular structure of the Cu complex immobilized on BPy-PMO-TMS after the reaction was investigated using elemental and XAFS analyses. Fig. 8a shows the Cu/BPy_{surf} and Cl/Cu molar ratios for Cu-BPy-PMO-TMS before and after reactions measured by EDX analysis. The Cu/BPy_{surf} ratios were almost constant before and after the reactions (approximately 0.2), which was consistent with the result that indicated almost no leaching of Cu species by the hot-filtration experiment. The Cl/Cu ratios were also almost constant

(approximately 1), which suggests that the coordination structure of Cu was not apparently changed after the reactions. The XAFS Fourier transforms before and after catalysis were almost identical, which suggests that the coordination structure around Cu was retained after the reaction (Fig. 8b).

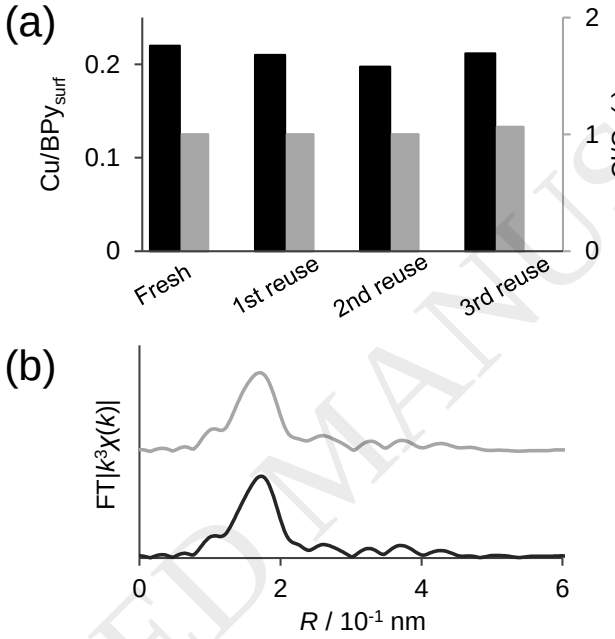

Fig. 8. (a) Cu/BPy$_{surf}$ ratio (black) and Cl/Cu ratio (grey) of Cu-BPy-PMO-TMS before and after the catalytic reactions. (b) Cu *K*-edge EXAFS Fourier transform (κ = 20-120 nm^{-1}) of Cu-BPy-PMO-TMS before (black line) and after the first reaction run (grey line).

3.3. Mukaiyama epoxidation in the presence of radical scavengers

The free radical auto-oxidation reaction occurs with Mukaiyama epoxidation at high substrate concentrations. Fig. 9a shows the time-dependent yield of **1** without a catalyst at high

concentrations of cyclohexene (7 mmol) and isobutyraldehyde (7 mmol). Epoxide **1** was produced after an induction period of 50 min and production increased steeply. After the reaction for 6 h, **1** was obtained in 23% yield with formation of by-products **2**, **3**, and **4** (Table 3). The selectivity of **1** relative to reaction products was decreased from 89% to 71% by increasing substrate concentrations in the absence of catalyst (vs. Table 2). A radical scavenger was added to the reaction mixture to control the free radical auto-oxidation. When 2,6-di-*tert*-butyl-*p*-cresol (BHT) was added into the reaction mixture as a molecular radical scavenger, the reaction was almost completely stopped and no product was afforded (Fig. 9a). This result indicates that the radical scavengers quench the radicals generated by auto-oxidation. During the investigation, auto-oxidation was also found to be quenched when PS-BPy beads were added into the reaction mixture. This suggests that PS-BPy also acts as a radical scavenger for Mukaiyama epoxidation.

Fig. 9b shows the time-dependent yield of **1** in the presence of the Cu-BPy-PMO-TMS catalyst at high concentrations of cyclohexene and isobutyraldehyde. Epoxide **1** was produced without the induction period and production increased at an almost constant rate. After the reaction for 6 h, 23% yield of **1** was obtained along with by-products **2**, **3**, and **4** (Table 3). By using Cu-BPy-PMO-TMS, the selectivity of **1** was increased to 79% even at high substrate concentrations. Then, BHT was added into the reaction mixture to control the free radical

auto-oxidation in the presence of the Cu-BPy-PMO-TMS catalyst. However, the reaction was almost completely stopped, similar to the auto-oxidation reaction without a catalyst. This result indicates that the molecular scavenger quenched the radicals generated in the solution and also in the mesopore spaces of Cu-BPy-PMO-TMS because the molecular scavenger can easily penetrate the mesochannels because of its molecular size (0.9 nm) is smaller than the pore diameter (3.8 nm).

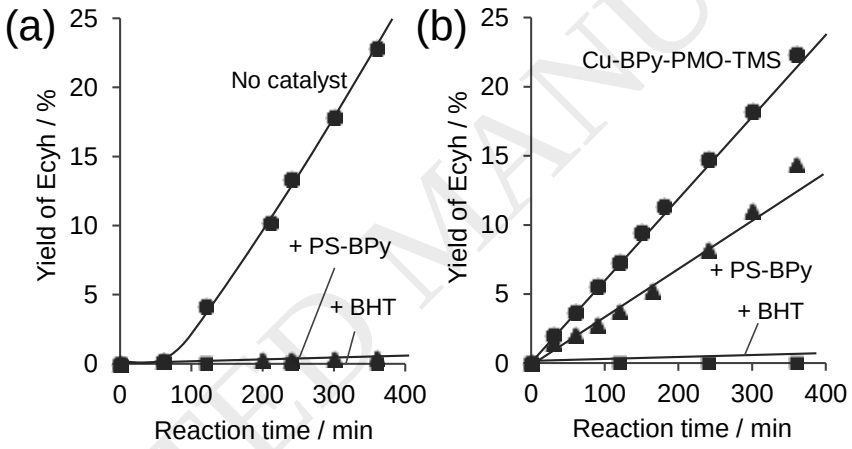

Fig. 9. Time dependent yield of **1** at high substrate concentration (7 mmol) without a catalyst (a, closed circles) and with the Cu-BPy-PMO-TMS catalyst (b, closed circles). A polymer radical scavenger (PS-BPy, closed triangles) or a molecular radical scavenger (BHT, closed squares) was added. All reactions were conducted with cyclohexene (7 mmol) and isobutyraldehyde (7 mmol) in chloroform (10 mL) at 40 °C under oxygen (1 atm).

However, when the solid scavenger PS-BPy was added into the reaction mixture, epoxide **1** was produced with a decrease in production rate to approximately 55% of the rate without a scavenger. After the reaction for 6 h, **1** was obtained in 15% yield along with by-products **2**, **3**, and **4** (Table 3). Although the selectivity of **1** was almost comparable to reaction system only using Cu-BPy-PMO-TMS, we clearly observed improved selectivity compared with blank reaction, possibly due to the suppression of undesired reactions such as radical-based allylic oxidation and ring opening reaction. Low product yield and low conversion of cyclohexene suggest that PS-BPy quenches the radicals in the solution but could not quench the reaction inside the mesopore spaces because the PS-BPy beads could not penetrate into the mesochannels. Thus, the combined use of Cu-BPy-PMO-TMS and PS-BPy enables the radical-based reaction to proceed solely inside the mesochannel spaces. The reaction is limited and controlled inside the mesochannels, which could be advantageous to achieve well-controlled radical reactions without thermal runaway, fire, or explosions.

Table 3. Product distributions of Mukaiyama epoxidation of cyclohexene without or with Cu – BPy-PMO-TMS at high substrate concentration.[a]

Catalyst	Conversion [%][b]	Selectivity [%][c]	Yield [%][d]	By-product selectivity [%][e]		
				2	**3**	**4**
Blank	32.5	70	23	4.0	10	15
Cu-BPy-PMO-TMS	29.0	79	23	1.6	9.0	10.4
Cu-BPy-PMO-TMS +PS-BPy	19.1	78	15	1.6	11.4	9.0

[a] All reactions were conducted with cyclohexene (7 mmol) and isobutyraldehyde (7 mmol) in chloroform (10 mL) at 40 °C under oxygen (1 atm). [b] Conversion of cyclohexene. [c] Selectivity of **1** was calculated as yield of **1**/total yield of reaction products. [d] Yield of **1** based on cyclohexene. [e] Selectivity of by-products was calculated as yield of **2** or **3** or **4**/total yield of reaction products, respectively.

4. Conclusion

Cu-bipyridine complexes were formed on the pore surfaces of BPy-PMO and BPy-PMO-TMS, and evaluated for catalysis of Mukaiyama epoxidation. BPy-PMO-TMS formed a Cu complex which is almost the same coordination structure as $Cu(bpy)Cl_2$, while BPy-PMO formed a mixture of the desired $Cu(bpy)Cl_2$ complex and an unidentified Cu species, possibly due to coordination with the surface silanol groups. Cu-BPy-PMO-TMS exhibited higher catalytic activity and recyclability for the epoxidation of cyclohexene with molecular oxygen than Cu-BPy-PMO. Auto-oxidation of cyclohexene occurred in the presence and absence of a catalyst at high substrate concentration. The addition of a solid radical scavenger could quench auto-oxidation in the solution but could not quench the reaction in the mesopore spaces of BPy-PMO. This result is very important because the combined use of a mesoporous catalyst and a solid scavenger enables radical-based reactions to proceed in a controllable manner and thus extends the scope of organic synthesis chemistry using radicals.

Conflicts of interest

There are no conflicts to declare.

Author information

Present Address

‡ S.I.: Kanagawa University, 3-27-1, Rokkakubashi, Kanagawa-ku, Yokohama 221-8686, Japan

Acknowledgements

The authors thank Ms Ayako Ohshima (Toyota Central R&D Laboratories, Inc.) for conducting the GC-MS analyses. This work was supported by the ACT-C program of the Japan Science and Technology Agency (JST) (grant number JPMJCR12Y1).

Appendix A. Supplementary data

Supplementary material related to this article can be found, in the online version.

References

[1] A. Studer, D. P. Curran, Angew. Chem. Int. Ed. 55 (2016) 58-102.

[2] M. L. You, M. Y. Liu, S. H. Wu, J. H. Chi, C. M. Shu, J. Therm. Anal. Calorim. 96 (2009)

777-782.

[3] W. C. Chen, C. M. Shu, Therm. Anal. Calorim. 126 (2016) 1937-1945.

[4] E. V. Ramos-Fernandez, N. J. Geels, N. R. Shiju, Green Chem. 16 (2014) 3358–3363.

[5] M. Waki, Y. Maegawa, K. Hara, Y. Goto, S. Shirai, Y. Yamada, N. Mizoshita, T. Tani, W. J. Chun, S. Muratsugu, M. Tada, A. Fukuoka, S. Inagaki, J. Am. Chem. Soc. 136 (2014) 4003-4011.

[6] Y. Maegawa, S. Inagaki, Dalton Trans, 44 (2015) 13007-13016.

[7] N. Ishito, H. Kobayashi, K. Nakajima, Y. Maegawa, S. Inagaki, K. Hara, A. Fukuoka, Chem. Eur. J. 21 (2015) 15564-15569.

[8] X. Liu, Y. Maegawa, Y. Goto, K. Hara, S. Inagaki, Angew. Chem. Int. Ed. 55 (2016) 7943-7947.

[9] K. Matsui, Y. Maegawa, M. Waki, S. Inagaki, Y. Yamamoto, Catal. Sci. Technol. 8 (2018) 534-539.

[10] S. Ishikawa, Y. Maegawa, M. Waki, S. Inagaki, ACS Catal. 8 (2018) 4160−4169.

[11] T. Yamada, T. Takai, O. Rhode, T. Mukaiyama, Chem. Lett. (1991) 1-4.

[12] T. Mukaiyama, T. Yamada, Bull. Chem. Soc. Jpn. 68 (1995) 17-35.

[13] W. Nam, H. J. Kim, S. H. Kim, R. Y. N. Ho, J. S. Valentine, Inorg. Chem. 35, (1996) 1045-1049.

[14] C. Detoni, N. M. F. Carvalho, R. O. M. A. Souza, D. A. G. Aranda, O. A. C. Antunes, Catal. Lett. 129 (2009) 79-84.

[15] S. R. Breeze, S. Wang, Inorg. Chem. 35 (1996) 3404-3408.

[16] H. Praliaud, S. Mikhailenko, Z. Chajar, M. Primet, Appl. Catal., B 16 (1998) 359-374.

[17] A. F. Stange, S. Tokura, M. Kira, J. Organomet. Chem. 612 (2000) 117−124.

[18] M. Hernández-Molinaa, J. González-Platalina, C. Ruiz-Péreza, F. Lloretb, M. Julveb, Inorg. Chim. Acta, 284 (1999) 258-265.

[19] A. Corma, M. Domine, J. A. Gaona, J. L. Jordá, M. T. Navarro, F. Rey, J. P. Pariente, J. Tsuji, B. M. Culloch, L. T. Nemeth, Chem. Commun. (1998) 2211-2212.

[20] M. Jia, A. Seifert, W. R. Thiel, Chem. Mater. 15 (2003) 2174-2180.

[21] H. Kochkar, F. Figueras, J. Catal. 171 (1997) 420-430.

[22] K. Nakatsuka, K. Mori, S. Okada, S. Ikurumi, T. Kamegawa, H. Yamashita, Chem. Eur. J. 20 (2014) 8348-8354.

[23] T. Kamegawa, A. Mizuno, H. Yamashita, Catal. Today 243 (2015) 153-157.